



Coil optimization of ultra-deep azimuthal electromagnetic resistivity logging while drilling tool based on numerical simulation

Zhengming Kang^{1,2} · Haojie Qin^{1,2} · Yi Zhang³ · Binbin Hou⁴ · Xiaolong Hao^{1,2} · Gang Chen^{3,5}

Received: 29 June 2022 / Accepted: 10 October 2022 / Published online: 21 October 2022
© The Author(s) 2022

Abstract

This paper presents a coil optimization method of the ultra-deep azimuthal electromagnetic (EM) resistivity Logging While Drilling (LWD) to obtain the best parameters of the tool for formation boundary detection by theory. First, a rapid numerical simulation algorithm, i.e. the Fast Hankel Transform (FHT) method, is developed to simulate the logging responses of the layered formation. A system of double inclined coils is selected based on the response characteristics and the depth of detection (DOD) from four common coils. Simulation results demonstrated that the optimal coils are perfectly suitable for anisotropic formation. Then, the crucial parameters of the frequency and spacing of the selected coils with a DOD of 30 m are determined using the Picasso diagram. In addition, the influences of the electrical parameter of the drilling collar and resistivity anisotropy of the formation on the response are investigated. The results show that the conductivity of the drilling collar, the thickness and the resistivity anisotropy of the formation all affect the DOD. Finally, formation models with different layers are created to verify the performance and signal intensity. The results demonstrate that the optimized coils not only have a large DOD but also possess a high signal intensity, further confirming the advantages of the preferred coils. Compared with the conventional physical experiment tests, the method of coil optimization proposed in this paper is more economical and efficient. The findings of this study can help better understand the detection characteristics of the different coils, which can provide theoretical support for designing and developing a tool with the best boundary capability.

Keywords Ultra-deep azimuthal EM resistivity · LWD · Coils optimization · DOD · Numerical simulation · Fast Hankel Transform · FEM

Abbreviations

Att	Amplitude ratio (dB)	DTB	Distance to boundary (m)
B	Magnetic induction intensity (Wb/m ²)	E	Electric field intensity (V/m)
D	Electric displacement vector (C/m ²)	EM	Electromagnetic
DDR	Deep directional resistivity	EMF	Electromotive force
DOD	Depth of detection (m)	<i>f</i>	Frequency (Hz)
		FEM	Finite element method
		FHT	Fast Hankel Transform
		<i>G</i>	Output function
		H	Magnetic field intensity (A/m)
		HA	High angle
		HD	High definition
		<i>H_v</i>	Filter response
		Hz	Horizontal
		Im	Imaginary part
		J	Conducted current density (A/m ²)
		<i>J_v</i>	Bessel function of the first kind of order <i>v</i>
		<i>k_ρ</i>	Integral variable
		<i>L</i>	Spacing (m)
		LWD	Logging while drilling
		M_S	Magnetic current

✉ Yi Zhang
yizhang86@163.com

¹ School of Electronic Engineering, Xi'an Shiyou University, Xi'an 710065, China

² Shaanxi Key Laboratory of Measurement and Control Technology for Oil and Gas Wells, Xi'an Shiyou University, Xi'an 710065, China

³ China Coal Technology and Engineering Group Corp, Xi'an Research Institute Co. Ltd, Xi'an 710077, China

⁴ Gas Production Plant 2 of Yanchang Gas Field, Shaanxi Yanchang Petroleum (Group) Co. Ltd, Xi'an 710085, China

⁵ School of Nuclear Science and Technology, Lanzhou University, Lanzhou 730000, China

n	Sampling points
p	Input function
PS	Phase difference ($^{\circ}$)
r	Integral variable
R	Receiver
Re	Real part
R_h	Horizontal resistivity ($\Omega\text{-m}$)
RSS	Rotary steerable system
R_v	Vertical resistivity ($\Omega\text{-m}$)
s	Integral variable
T	Transmitter
TI	Transversely isotropic
TVD	True vertical depth (m)
V	EMF signal (nV)
α	Deviated angle of the well ($^{\circ}$)
Δ	Sampling interval
ϵ	Dielectric constant of the medium (F/m)
ϵ_r	Relative permeability of the drilling collar
λ	Variable
λ^2	Resistivity anisotropy coefficient (R_v/R_h)
μ	Permeability of the medium (H/m)
μ_0	Magnetic permeability in vacuum (H/m)
π	Hertz vector potential
ρ	Charge density (C/m^3)
$\bar{\sigma}$	Conductivity tensor (S/m)
σ_c	Conductivity of the drilling collar (S/m)
σ_h	Horizontal conductivity (S/m)
σ_v	Vertical conductivity (S/m)
Ψ	Scalar potential (V)
ω	Angular frequency (rad/s)

Introduction

With the demand for efficient development technology in the exploration of complex oil and gas reservoirs, directional drilling technologies are widely used in HA/Hz wells. Directional drilling can efficiently increase production and reduce cost. The EM resistivity logging technology plays a crucial role in geological guidance and formation evaluation in directional drilling. It can provide information about the formation boundary and the oil–water boundary, which helps to reduce the uncertainty of well placement within the sweet-spot of a reservoir (Rabinovich et al. 2011; Wu et al. 2013; Li et al. 2018). However, because of the smaller DOD (less than 6 m) of the conventional azimuth EM resistivity LWD tools, its application to the evaluation of far boundaries in complex reservoirs is limited.

In recent years, many oil service companies have been committed to the development of LWD tools for deeper DOD (Li et al. 2005; Pamler et al. 2008; Bittar et al. 2007; Wei et al. 2012), i.e. ultra-deep azimuthal EM resistivity LWD tools. For instance, Schlumberger launched the deep

vision resistivity (VDR) tool, PeriScope High Definition (HD), and deep directional resistivity (DDR) tools (Omeragic et al. 2005; Oystein et al. 2014; Hartmann et al. 2014). VDR does not have azimuthal capability, PeriScope HD and DDR have large spacing between the transmitter and receiver, ultra-deep measurement depth and azimuthal capability, and the theoretical DOD can exceed 30 m. In addition, they have real-time imaging function at multi-boundary and specific look-ahead capability. Schlumberger launched the first commercial ultra-deep azimuth EM resistivity tool geosphere shortly after launching DDR. It consists of a set of transmitters and two sets of receivers. In addition, due to the multi-frequency and multi-spacing measurement methods, the tool can detect the boundary of formation with multiple DODs (Seydoux et al. 2014; Thiel and Dzevat 2018). Afterwards, Baker Hughes launched Visitrak, which provides multi-boundary real-time imaging and performs ultra-deep investigation of formation boundary. However, its capability of looking ahead is insufficient. Halliburton launched a new generation EarthStar tool in 2018, and the field test of the carbonate reservoir in the North Sea region shows that the DOD can be as high as 60 m (Wu et al. 2018).

These EM resistivity LWD tools have a similar measurement principle, while the coil combination, measurement frequency, and tool length are different. There are many tool parameters that affect the DOD of a tool, such as the frequency, the spacing, and the inclination angle between the transmitter and receiver. When designing a new tool, it is challenging to select a set of proper parameters with current technology. To solve this problem, the effects of the response on the tool are usually discussed by numerical simulations before optimizing the parameters of the tool. There are many related studies focused on it. Li et al. (2020b) used grey relational analysis to quantify the influence of tool parameters on the measurement voltage and the DOD. They also used the random forest to fit data and identify an optimal combination of tool parameters. Wu et al. (2020) quantitatively analysed the effect of anisotropy on tool responses and data processing. They investigated the sensitivity of tool to electric anisotropy and inversion accuracy. Zhang et al. (2021) proposed a sensitivity function to describe the measurement properties of azimuth, dipping angle, and resistivity. They also optimized the operating frequency and spacing under different formation resistivity conditions. However, the coil types used in above literature were only one, namely one axial coil as transmitter and one inclined coil as receiver. In fact, there are still three types of coils, i.e. the axial or inclined coil as the transmitter, and the radial or inclined coil as the receiver, which receives less attention. Meanwhile, the formation models are limited when optimizing the parameters of the frequency and spacing, which makes the structure parameters of the tool suitable for the limited formations. Thus, systematic research of coils optimization

by theory is essential. The simulation results can help to design a suitable combination of coils, improve the boundary detection distance of the logging tool, and shorten the tool length (Zhang et al. 2008; Wang 2008).

In drilling activities, when the tool can detect the formation boundary 30 m away from the borehole, it is considered to be better able to perform reservoir navigation. Therefore, this paper aims to optimize tool parameters with a DOD of 30 m. First, the principle of the ultra-deep azimuthal EM resistivity LWD tool is introduced. Then, the FHT method is developed to speed up the numerical program. After that the structure and parameters of a coil that can achieve a deeper DOD are optimized by comparing the detection performance of different coil combinations, and the influence of the drilling collar parameters and formation parameters on the logging response is evaluated. Finally, the response performance of the optimized coils is simulated in formation models with different boundaries. The results reveal that the selected coils have a large DOD and a strong measurement signal. The conclusions could provide theoretical support for developing the ultra-deep azimuthal EM resistivity LWD tool.

Principle of ultra-deep azimuthal EM resistivity LWD tool

Traditional EM resistivity LWD tools use axial coils and the measurement results are superposition of the resistivity of the formation around the borehole, without the ability of azimuthal resistivity detection (Wei et al. 2010). To improve the tool's capability, the novel tool adds an inclined coil and a radial coil to the traditional axial coil, which is able to distinguish the direction. Commercial tools consist mainly of four combinations (Li et al. 2020b) shown in Fig. 1 (T represents transmitter and R represents receiver).

For type I, the measurement signals are all from the boundary. Namely, there will be no signal if the formation is homogeneous. The measured induced electromotive force (EMF) signals are usually used to characterize the distance between the tool and the formation boundary. The

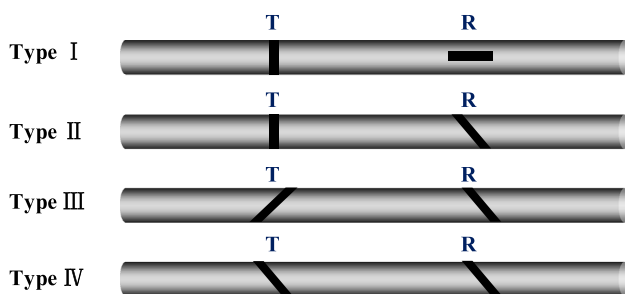


Fig. 1 Schematic diagram of different coil combinations

measurement EMFs of the other three coils are both from the boundary and from the formation in which the tool is located. So, the boundary information is often expressed as the ratio of two measurements at different azimuth angles to eliminate the effect of the formation in which the tool works. Taking type II as an example, it is composed of an axial transmitter T and an inclined receiver R. The EMF of the receiver is measured when the tool rotates along the axis to different azimuth angles, i.e. α_1 and α_2 . Then, the EMF is converted into amplitude ratio and phase difference geological signals to indicate the boundary information (Rabinovich et al. 2012):

$$\text{Att} = 20 \log_{10} \frac{\sqrt{[\text{Re}(V_{\alpha_1})]^2 + [\text{Im}(V_{\alpha_1})]^2}}{\sqrt{[\text{Re}(V_{\alpha_2})]^2 + [\text{Im}(V_{\alpha_2})]^2}} \quad (1)$$

$$\text{PS} = \tan^{-1} \frac{\text{Im}(V_{\alpha_1})}{\text{Re}(V_{\alpha_1})} - \tan^{-1} \frac{\text{Im}(V_{\alpha_2})}{\text{Re}(V_{\alpha_2})} \quad (2)$$

where V is the EMF signal of the receiver. Re and Im denote the real and imaginary part of V , respectively. α_1 and α_2 are usually set to 0° and 180° . Att and PS signify the amplitude ratio geological signal and the phase difference geological signal, respectively.

The vertical distance from the measured point to the formation boundary is usually termed DTB, as shown in Fig. 2. Depth of detection (DOD) refers to the maximum DTB that the tool can detect when it is parallel to the formation boundary in the two-layer formation model (Wang 2018). DOD is the most crucial parameter of the ultra-deep azimuthal EM resistivity LWD tool. For type I, the threshold of DOD is defined as 10 nv, which represents that there exists a formation boundary along the drilling direction. In other words, the formation boundary can be detected when the EMF is higher than the defined threshold. For the other types, the thresholds of Att and PS are defined as 0.03 dB and 0.3° , respectively.

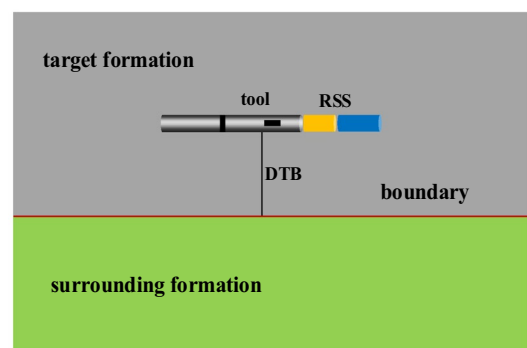


Fig. 2 Schematic diagram of DOD definition

Numerical simulation method

Common numerical simulation methods consist of analytical solution, finite element method (FEM) and finite difference methods. They are suitable for different formation models. For instance, the analytical method can quickly calculate the logging responses of a one-dimensional formation model, so it is widely used in real-time inversion. When the formations model is complex, the three-dimensional finite difference and three-dimensional FEM should be considered.

To simplify the formation model, the horizontally layered formation model is developed. For transversely isotropic (TI) formation, the propagation coefficient matrix method can effectively avoid the simultaneous solution of 2 N equations by the N-layer boundary. When there are many formation boundaries, the calculation speed of this recursive method is faster. This paper adopts this method to calculate the measurement response of the TI model.

The propagation of electromagnetic waves in one medium satisfies Maxwell's equations in differential form:

$$\begin{cases} \nabla \times \mathbf{H} = \mathbf{J} + \frac{\partial \mathbf{D}}{\partial t} \\ \nabla \times \mathbf{E} = -\frac{\partial \mathbf{B}}{\partial t} \\ \nabla \cdot \mathbf{B} = 0 \\ \nabla \cdot \mathbf{D} = \rho \end{cases} \tag{3}$$

where \mathbf{H} is the magnetic field intensity, \mathbf{E} denotes the electric field intensity, \mathbf{B} represents the magnetic induction intensity, \mathbf{D} is the electric displacement vector, and \mathbf{J} is the conducted current density. ρ signifies the charge density.

The electromagnetic wave in the medium satisfies the constitutive relation:

$$\begin{cases} \mathbf{D} = \epsilon \mathbf{E} \\ \mathbf{B} = \mu \mathbf{H} \\ \mathbf{J} = \tilde{\sigma} \cdot \mathbf{E} \end{cases} \tag{4}$$

where ϵ is the dielectric constant of the medium. μ denotes the permeability of the medium, and $\tilde{\sigma}$ indicates the conductivity tensor.

The transmitter can be simplified as a magnetic dipole source. The harmonic current source $e^{-i\omega t}$ is generally used in the ultra-deep EM resistivity LWD method.

In cylindrical coordinates, the Maxwell equations can be written in matrix form:

$$\begin{bmatrix} 0 & -\frac{\partial}{\partial z} & \frac{1}{\rho} \frac{\partial}{\partial \varphi} \\ \frac{\partial}{\partial z} & 0 & -\frac{\partial}{\partial \rho} \\ -\frac{1}{\rho} \frac{\partial}{\partial \varphi} & \frac{1}{\rho} + \frac{\partial}{\partial \rho} & 0 \end{bmatrix} \begin{bmatrix} E_\rho \\ E_\varphi \\ E_z \end{bmatrix} = i\omega\mu \begin{bmatrix} H_\rho \\ H_\varphi \\ H_z \end{bmatrix} \tag{5}$$

$$\begin{bmatrix} 0 & -\frac{\partial}{\partial z} & \frac{1}{\rho} \frac{\partial}{\partial \varphi} \\ \frac{\partial}{\partial z} & 0 & -\frac{\partial}{\partial \rho} \\ -\frac{1}{\rho} \frac{\partial}{\partial \varphi} & \frac{1}{\rho} + \frac{\partial}{\partial \rho} & 0 \end{bmatrix} \begin{bmatrix} H_\rho \\ H_\varphi \\ H_z \end{bmatrix} = \begin{bmatrix} \sigma_h & 0 & 0 \\ 0 & \sigma_h & 0 \\ 0 & 0 & \sigma_v \end{bmatrix} \begin{bmatrix} E_\rho \\ E_\varphi \\ E_z \end{bmatrix} \tag{6}$$

where E_ρ, E_φ and E_z are the components of \mathbf{E} , respectively, and H_ρ, H_φ and H_z are the components of \mathbf{H} , respectively. ω represents the angular frequency. μ_0 signifies magnetic permeability in vacuum. σ_h and σ_v denote the horizontal and vertical conductivity, respectively.

Equations (7) and (8) can be obtained by converting Eqs. (5) and (6):

$$\begin{bmatrix} E_\rho \\ E_\varphi \end{bmatrix} = \frac{1}{\lambda^2 k_\rho^2} \begin{bmatrix} 0 & -1 \\ 1 & 0 \end{bmatrix} \begin{bmatrix} \frac{1}{\rho} \frac{\partial^2}{\partial z \partial \varphi} \\ \frac{\partial^2}{\partial z \partial \rho} \end{bmatrix} E_z + \frac{i\omega\mu}{k_\rho^2} \begin{bmatrix} \frac{1}{\rho} \frac{\partial}{\partial \varphi} \\ -\frac{\partial}{\partial \rho} \end{bmatrix} H_z \tag{7}$$

$$\begin{bmatrix} H_\rho \\ H_\varphi \end{bmatrix} = \frac{1}{k_\rho^2} \begin{bmatrix} 0 & -1 \\ 1 & 0 \end{bmatrix} \begin{bmatrix} \frac{1}{\rho} \frac{\partial^2}{\partial z \partial \varphi} \\ \frac{\partial^2}{\partial z \partial \rho} \end{bmatrix} H_z + \frac{\sigma_h}{\lambda^2 k_\rho^2} \begin{bmatrix} \frac{1}{\rho} \frac{\partial}{\partial \varphi} \\ -\frac{\partial}{\partial \rho} \end{bmatrix} E_z \tag{8}$$

where λ and k_ρ are variables.

As can be seen from Eqs. (7) and Eq. (8), only the vertical component of the electromagnetic field is required in each layer of the TI model. The horizontal component can be obtained from Eqs. (7) and (8), so the solution can be obtained for the whole wave field.

In anisotropic formations, the Maxwell equations of the time-harmonic field can be expressed as:

$$\begin{cases} \nabla \times \mathbf{H} = \tilde{\sigma} \cdot \mathbf{E} \\ \nabla \times \mathbf{E} = i\omega(\mu_0 \mathbf{H} + \mu_0 \mathbf{M}_s) \end{cases} \tag{9}$$

$$\tilde{\sigma} = \begin{bmatrix} \sigma_h & 0 & 0 \\ 0 & \sigma_h & 0 \\ 0 & 0 & \sigma_v \end{bmatrix} \tag{10}$$

where \mathbf{M}_s indicates the applied magnetic current,

The Hertz potential theory is often used in the derivation, and the Hertz vector potential π and the scalar potential Ψ satisfy:

$$\begin{cases} \tilde{\sigma} \cdot \mathbf{E} = i\omega\mu_0\sigma_h \nabla \times \pi \\ \mathbf{H} = i\omega\mu_0\sigma_h \pi + \nabla \Psi \\ \nabla \cdot (\sigma \cdot \pi) = \sigma_v \Psi \end{cases} \tag{11}$$

By substituting Eq. (11) into Eq. (9), the expression of the magnetic dipole source in uniformly anisotropic media can be obtained, and it can be transformed into the cylindrical coordinate system as:

$$\begin{cases} \pi_\rho = \frac{1}{4\pi}(M_x \cos \alpha + M_y \sin \alpha) \int_0^\infty i \frac{J_0(k_\rho \rho)}{\lambda k_{v,z}} e^{i\lambda|z|k_{v,z}k_\rho} dk_\rho \\ \pi_\phi = \frac{1}{4\pi}(-M_x \sin \alpha + M_y \cos \alpha) \int_0^\infty i \frac{J_0(k_\rho \rho)}{\lambda k_{v,z}} e^{i\lambda|z|k_{v,z}k_\rho} dk_\rho \\ \pi_z = \frac{M_z}{4\pi} \int_0^\infty ik_\rho \frac{J_0(k_\rho \rho)}{\lambda k_{h,z}} e^{i\lambda|z|k_{h,z}} dk_\rho + \\ \frac{1}{4\pi}(M_x \sin \alpha + M_y \cos \alpha) \int_0^\infty iz \frac{J_0(k_\rho \rho)}{\rho} \left[\frac{\lambda}{k_{v,z}} e^{i\lambda|z|k_{v,z}} - \frac{1}{k_{h,z}} \right] k_\rho dk_\rho \end{cases} \quad (12)$$

where π_ρ , π_ϕ , and π_z are the component of the π . M_x, M_y , and M_z denote the components of M_s . $k_{h,z}$ and $k_{v,z}$ are the components of k . α indicates deviated angle of the well. J_0 and J_1 signify the Bessel function of the first kind of order 0 and Bessel function of the first kind of order 1, respectively.

Substitute Eq. (12) into Eq. (11) to obtain:

$$\begin{cases} E_z = -\frac{1}{4\pi}(M_x \sin \alpha - M_y \cos \alpha) \int_0^\infty \omega \mu \lambda k_\rho^2 i \frac{J_1(k_\rho \rho)}{k_{v,z}} e^{i\lambda|z|k_{v,z}k_\rho} dk_\rho \\ H_z = \frac{1}{4\pi}(M_x \cos \alpha + M_y \sin \alpha) \int_0^\infty k_\rho^2 \frac{\partial|z|}{\partial z} J_1(k_\rho \rho) e^{i\lambda|z|k_{v,z}} dk_\rho + \frac{M_z}{4\pi} \int_0^\infty ik_\rho^3 \frac{J_0(k_\rho \rho)}{k_{h,z}} e^{i\lambda|z|k_{h,z}} dk_\rho \end{cases} \quad (13)$$

where k_ρ is an integral variable.

The above formula reveals that the field can be expressed in the integral form of the Bessel function. However, the speed of direct calculation of the integral formula is slow. The FHT is often used to speed up the numerical calculation. The continuous function $g(r)$ can be expressed as (Anderson 1979; Johansen and Sørensen 1979; Gao et al. 2013):

$$g(r) = \int_0^\infty f(s)J_\nu(sr)ds \quad (14)$$

where $f(s)$ is the integral kernel function. $J_\nu(sr)$ denotes the Bessel function of the first kind of order ν . s and r are the integral variables.

The Hankel transformation of s and r are given by:

$$\begin{cases} s = e^{-y} \\ r = e^{-x} \end{cases} \quad x, y \in (-\infty, +\infty) \quad (15)$$

where x and y are new variables in Hankel transform.

By substituting Eq. (14) into Eq. (15), the following equation can be obtained:

$$e(x)g(e(x)) = \int_{-\infty}^{+\infty} p(e(y))[J_\nu(e(x-y))e(x-y)]dy \quad (16)$$

Let $G = e^x g(e^x)$ and $H_\nu(y) = e^y J_\nu(e^y)$, then:

$$G = \sum_{n=-\infty}^\infty p(n\Delta)H_\nu \quad (17)$$

where H_ν is the filter response. p represents the input function. n denotes the sampling points. G indicates the output function, and Δ signifies the sampling interval.

After the change, the summation of product operations is only required, which dramatically reduces the number of operations and increases the calculation speed. With a single calculation, the filter coefficient can be determined. The algorithm is accurate, fast, and relatively stable. It is suitable for horizontally layered formation. In this paper, FEM is used considering the influence of the tool structure, such as drilling collar.

Parameters affecting the logging response

Coil type optimization

Based on the FHT method, the two-layer isotropic formation model and the three-layer formation model with anisotropy formation in the middle layer are developed to investigate the detection characteristics of four types of coils (Fig. 3). In the model, the well deviation angle is set to 85°, almost equivalent to the horizontal well.

Coil type I uses the measured EMF signal to directly reflect the formation boundary, while the other three coils use Att and PS to define the boundary signals. Figure 4 presents the logging response characteristics of type I at different frequencies (10 and 20 kHz), with a spacing of 5 m. When comparing the logging responses with frequencies of 10 and 20 kHz, it can be seen that the greater the frequency is, the greater the EMF and the DOD are.

By counting the DODs under all combinations of the parameter, it is deduced that the calculated DOD is less than 30 m in a well with a deviation angle of 85°, shown in Table 1. Therefore, it is difficult for coil I to achieve a higher DOD when the measured voltage threshold is 10 nv. So far, 10nv is almost the smallest signal that the LWD tool can detect. Moreover, since coil I uses the true value of the EMF to scale the tool, the calibration algorithm is more complex than the other coils. Therefore, we can draw the conclusion that coil I is not the best scheme with a DOD of 30 m. In addition, if the signal-to-noise ratio of

Fig. 3 Schematic diagram of the formation models. **a** Two-layer isotropic formation; **b** three-layer anisotropic formation

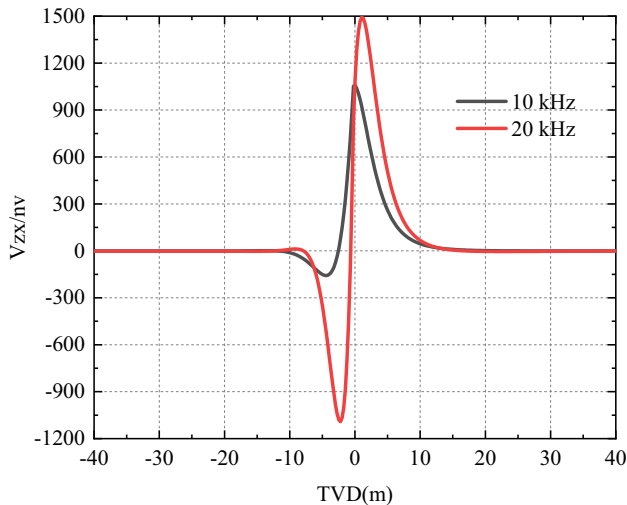
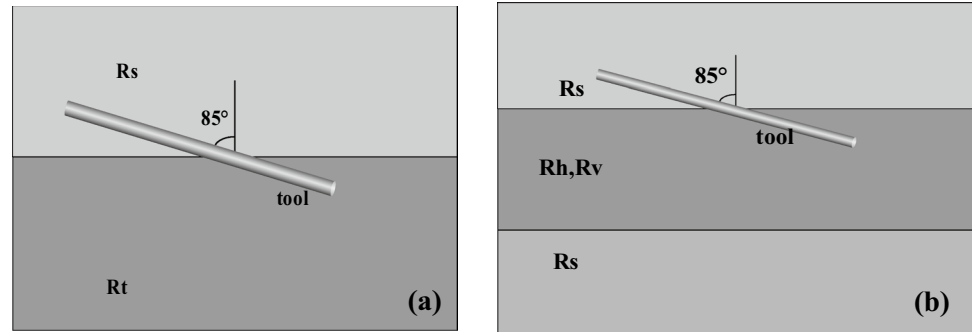


Fig. 4 Logging response of coil I in two-layer formation model

the measurement signal can be improved, the threshold of the EMF can be appropriately reduced, and coil I is expected to achieve longer DOD in the future.

Using the model in Fig. 3a, the Att and PS responses of the other three coils are simulated, and the DODs of the three coils are compared to each other. The results are shown in Fig. 5. It reveals that the DOD corresponding to Att and PS of coil II and coil III (i.e. double inclined coil) is obviously greater than coil IV. The DODs of Att and PS are listed in Table 2. It can quantitatively explain the disadvantages of type IV. Simultaneously, after analysing the

Table 1 DODs of type I under different frequencies and spacings

f (kHz)	L (m)	DOD (m)
100	2.5	17.73
50	5	21.93
100	5	18.13
10	10	25.54
20	10	22.93
50	10	23.13
10	20	26.94
20	20	22.53

EMF when coil IV passes through the formation boundary, it is deduced that the positive or negative voltage values have not changed, revealing that it cannot indicate the drilling direction whether the tool is up or down. Therefore, coil IV should be abandoned. Table 2 also shows that the DODs of PS between type II and type III are close. For Att signals, the DOD of type III is slightly better than that of type II. Compared with coil II, the response horn of coil III has a good correspondence with the formation boundary, which is beneficial to data inversion.

To further compare the investigation performance of coil II and coil III, the logging response characteristics of the two type coils in the three-layer anisotropic formation model are simulated. The model used here is illustrated in Fig. 3b. The resistivity of the upper and lower formations is isotropic, and the middle formation is anisotropic. The boundaries of the formation are at -5 and 5 m. The results are presented in Fig. 6. Compared with coil II, coil III has larger signal intensity, and it more accurately reflects the formation boundary, helping to accurately invert the formation boundary. In other words, coil III is less affected by resistivity anisotropy than type II. Therefore, coil III is a better scheme and is selected the optimized coils. The following contents will determine the optimal frequency and spacing of coil III. In addition, the influence of the tool parameters and formation parameters will also be analysed.

Parameters determination of the optimal coil

The frequency and spacing are the two most critical parameters of the tool that affect the DOD. When designing a tool, the DODs of Att and PS are determined by calculating its corresponding responses at different frequencies, spacing and resistivity of formation (Iverson 2004; Prensky 2006). In addition, it is necessary to avoid the tool length being too long. Therefore, a method should be proposed to quantify the DOD under different combinations of frequency and spacing to determine the two parameters. Unfortunately, there is no effective method to optimize these two parameters. The traversal method is a good choice for parameter selection and it is used in this paper. The FHT algorithm is used to

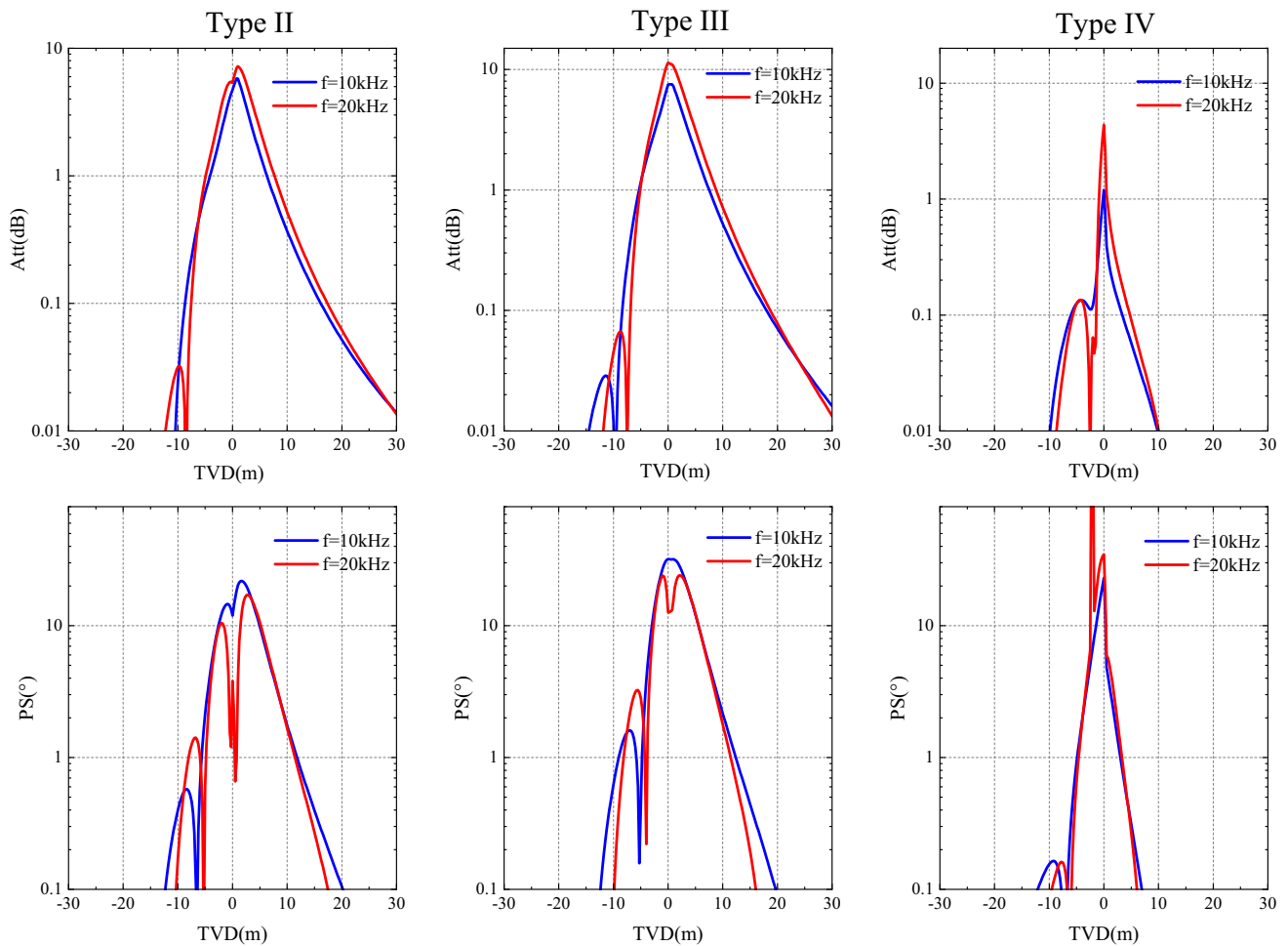


Fig. 5 Comparison of logging response of the three coils at different frequencies

Table 2 DODs of three coils under different frequencies and spacings

Geological signal	f (kHz)	DODs of coils(m)		
		Type II	Type III	Type IV
Att	10	23.75	25.45	6.85
	20	24.25	25.35	7.72
PS	10	16.15	16.35	5.12
	20	14.15	14.75	4.85

iteratively calculate the DODs of Att and PS corresponding to different frequencies, spacings and formation resistivity. The model here is the same as in Fig. 3a.

Figures 7 and 8 present the results of the traversal calculation, which is also called the Picasso diagram. In Fig. 7a, b, c and d is the DODs of Att, respectively, corresponding to resistivity ratio (Rt/Rs) of the two-layer formation are 5, 10, 30 and 50. In Fig. 8a, b, c and d is the DOD of the PS corresponding to resistivity ratios of 5, 10, 30 and 50, respectively. It is noted that the resistivity range of the

selected formation is wider to make the optimized coils suitable for most formations. It demonstrates that the relationship between the frequency, spacing and DOD is not linear or monotonous. The lower the frequency and the larger the spacing signify the larger DOD. The higher the contrast of the formation resistivity, the higher the DOD corresponding to the same frequency and spacing. That is, the DOD of Att and PS signals under the same frequency and spacing are also different. Therefore, it is necessary to take into account the contrast of the formation resistivity.

There are three principles that must be observed in the procedure of selecting parameters (frequency and spacing). First, the spacing should be as short as possible to make the tool have a low production cost and be easy to operate in drilling activities. Second, the frequency should be higher so that measurement signals can be detected. The last is that both the DOD of Att and the DOD of PS are required to be more than 30 m. Based on these principles, the Picasso diagrams are searched for finding the proper frequency and spacing under different resistivity ratios. Through computing

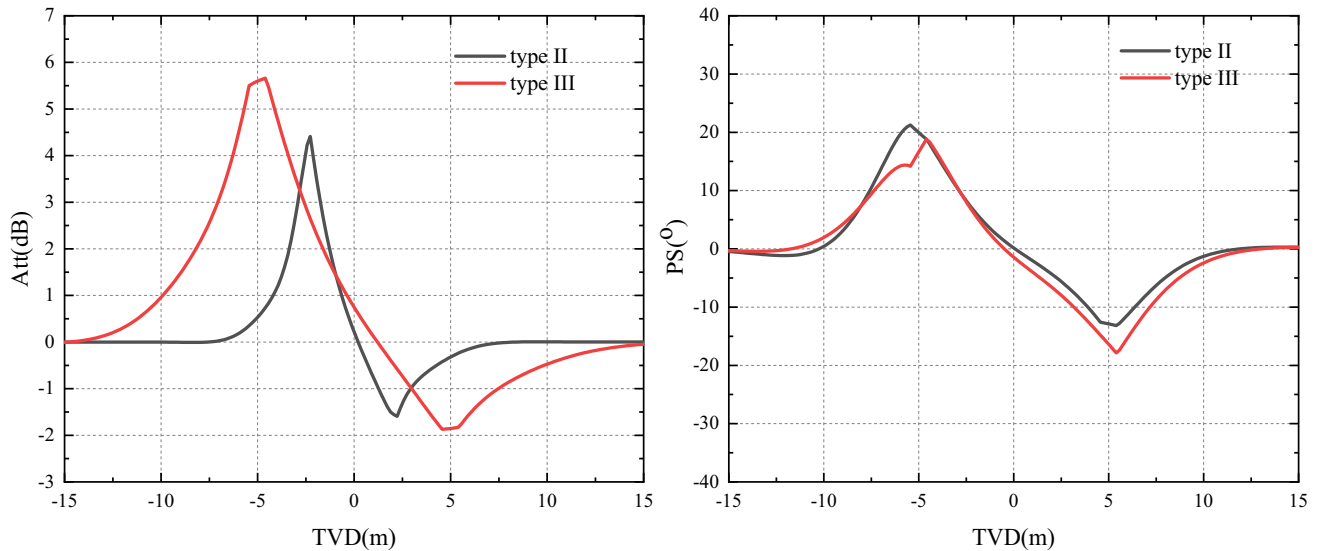
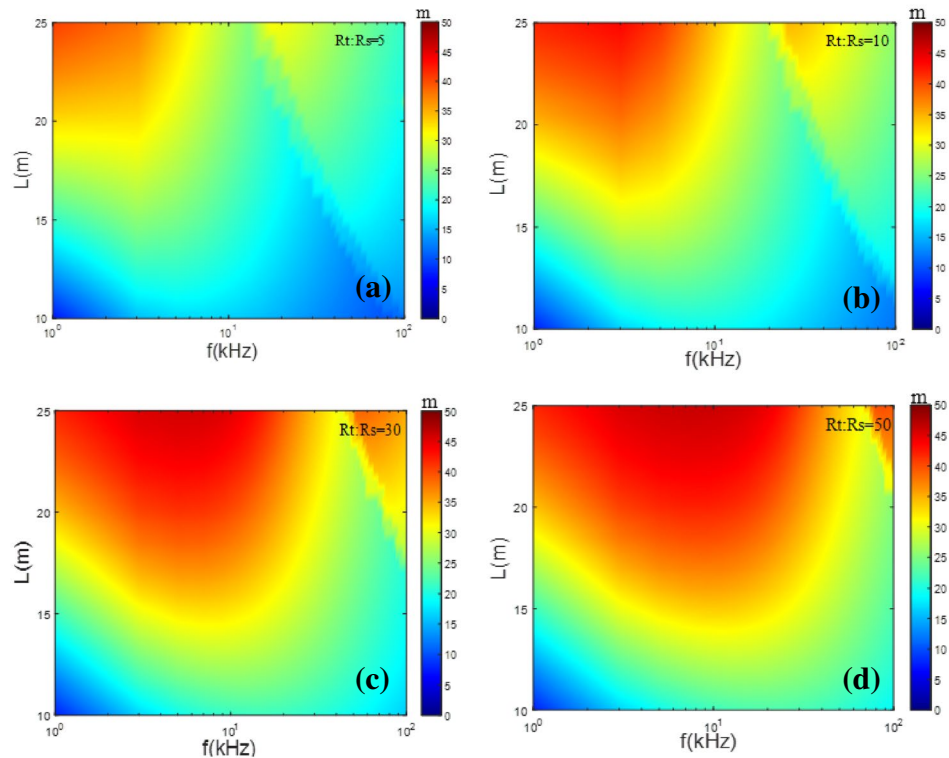


Fig. 6 Logging responses of coil types II and III in anisotropic formation model

Fig. 7 DODs of Att under different frequencies and spacings



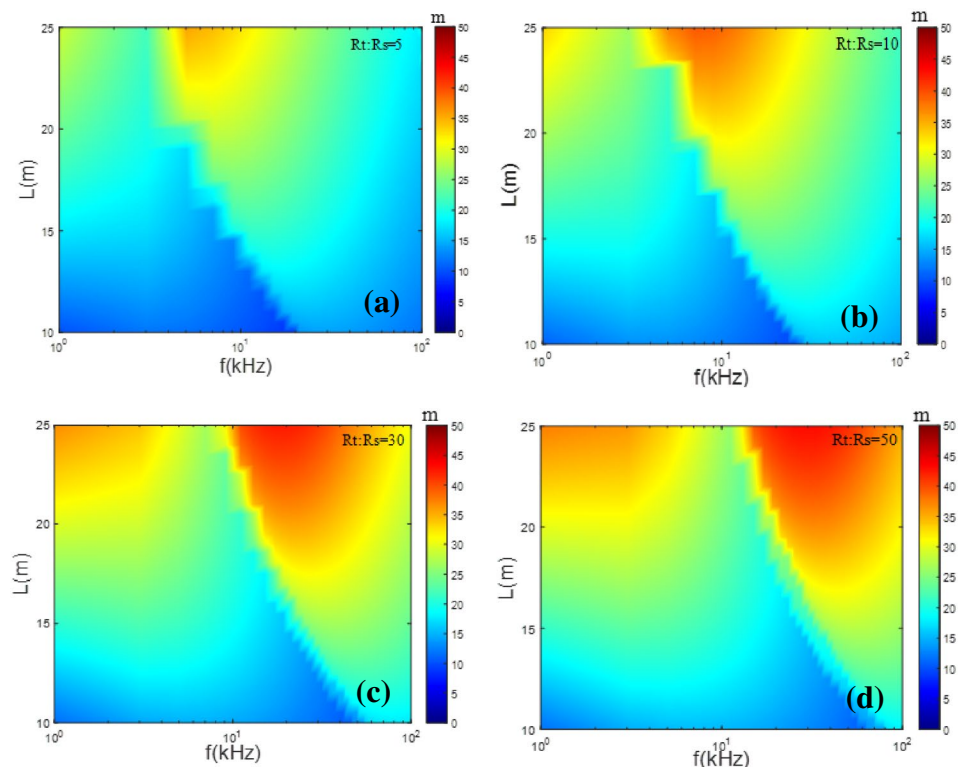
the entire models, when the frequency is 10 kHz and the spacing is 20 m, DOD index of 30 m can be satisfied under most formation models.

The influencing factors of the optimized coils

(1) Conductivity of the drilling collar.

In tool manufacturing, the selection of the drilling collar material has a specific effect on the measurement results. To quantify this factor, a formation model with drilling collar is developed using commercial FEM simulation software, i.e. COMSOL Multiphysics. The influence of the drilling collar's conductivity on the measurement signal is first investigated. Four formation resistivity, i.e. 1, 10, 100, and 1000 Ω -m, is considered. The conductivity of the drilling collar

Fig. 8 DODs of PS under different frequencies and spacings



varies from 10^2 to 10^9 S/m, and the relative permeability of the drilling collar is 1. In Fig. 9a, b, c, and d represents the four cases of formation resistivity mentioned above, respectively. It shows that the real part and imaginary part of the measured EMF change as the formation resistivity varies when the conductivity of the drilling collar is lower than 10^6 S/m. The EMFs obtained under different formation resistivity remain unchanged when the conductivity of drilling collar is greater than 10^6 S/m. Therefore, the conductivity of the drilling collar should be controlled to be greater than 10^6 S/m in actual production, which can ensure that the influence of the drilling collar on the measurement signal is a fixed value, and the deduction of the influence of the drilling collar is relatively simple.

(2) Permeability of the drilling collar.

Permeability is another parameter of the drilling collar. Under the same FEM model as in Fig. 9, the influence of the drilling collar's permeability on the measurement signal is studied. The resistivity of the formation is $1 \Omega\cdot\text{m}$, and the relative permeability of drilling collar is considered as 1, 10, 100, 1000, 10,000, and 1,00,000, respectively. Figure 10 shows the influence of different drilling collar's permeability on the EMF. It demonstrates that the permeability almost does not affect the measured signal. Therefore, the

permeability of the drilling collar can be flexibly selected according to specific conditions.

(3) Thickness of the formation.

The three layers formation model shown in Fig. 3b is used to simulate the influence of the formation thickness. The resistivity is isotropic, and the resistivity of the three-layer formation is 2, 20, and $2 \Omega\cdot\text{m}$, respectively. The middle layer is termed target layer. The thickness of the target layer is 10, 20, 30, 40, 50, and 60 m, respectively. The deviation angle of the well is 85° , and the formation model is symmetrical at $\text{TVD}=0$. It depicts from Fig. 11 that the DODs of Att and PS are affected by the formation thickness when the formation thickness is lower than the maximum DOD (about 30 m) of the tool. Additionally, the maximum DOD is half of the target layer thickness and is affected by the double boundary. As the thickness of the target layer gradually increases to the maximum DOD of the tool, the mutual influence of the two boundaries disappears.

(4) Resistivity anisotropy of the formation.

The influence of the resistivity anisotropy is also investigated by the model in Fig. 3b. The thickness of the middle layer is 50 m to eliminate the thickness effect. Its vertical

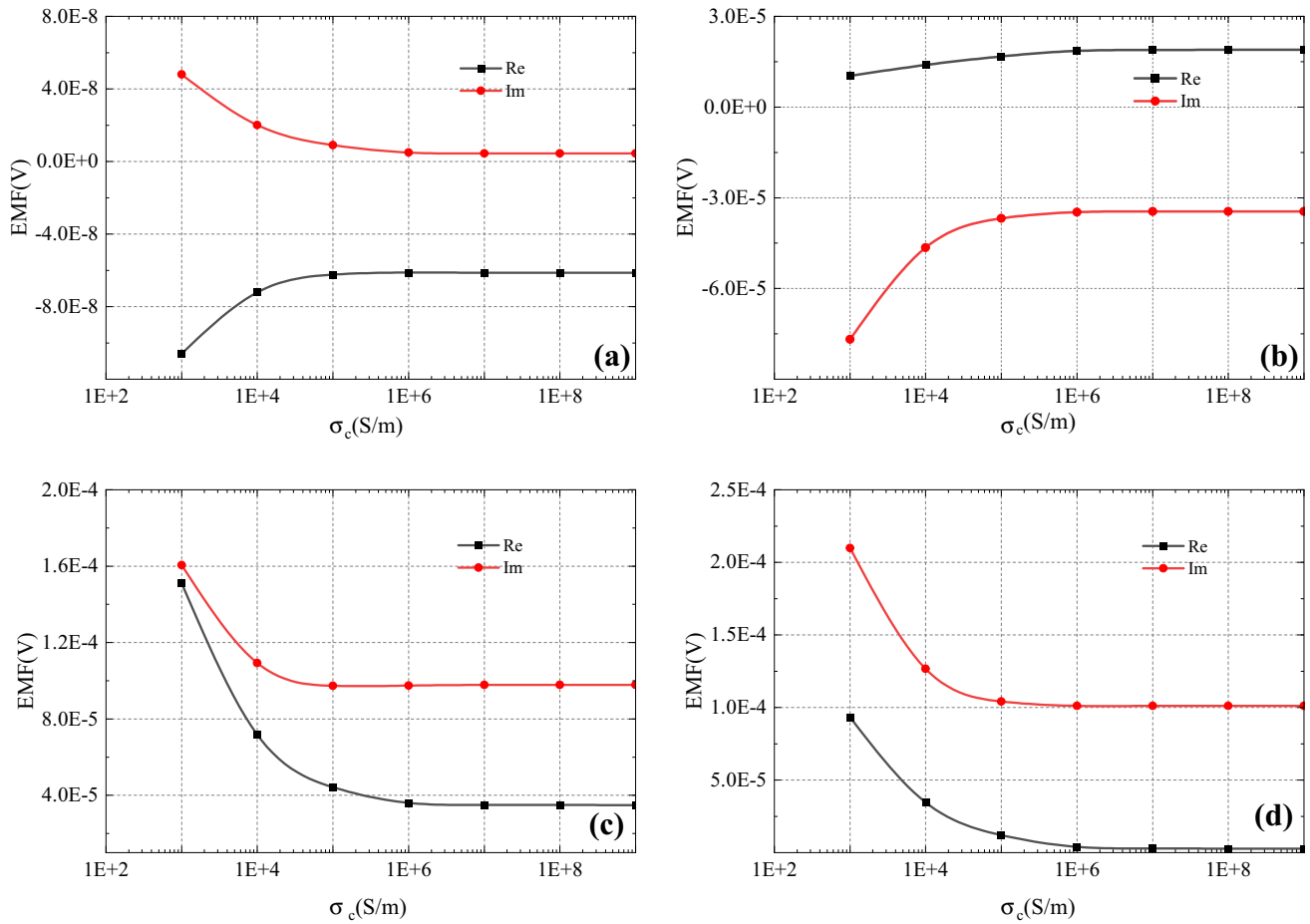


Fig. 9 Influence of the drilling collar’s conductivity on EMF

resistivity R_v is $20 \Omega\cdot m$ and its horizontal resistivity R_h is 20, 10, and $4 \Omega\cdot m$, respectively. That is, the resistivity anisotropy coefficient ($\lambda^2 = R_v/R_h$) equals 1, 2, and 5,

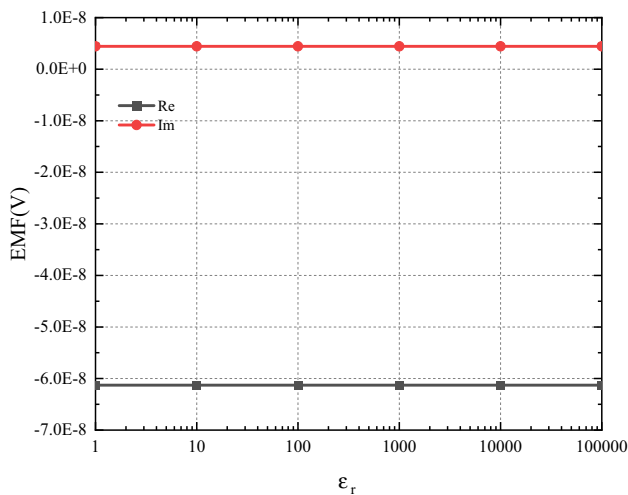


Fig. 10 Influence of the relative permeability of the drilling collar on EMF

respectively. The resistivity of the upper and lower surrounding rocks is isotropic and equal to $2 \Omega\cdot m$. Figure 12 indicates that the horns of Att and the PS cure appear at the same TVD in different λ^2 . However, the larger the λ^2 , the lower the measured Att and PS signal. That is, the smaller the DOD of the tool is. Therefore, the anisotropy of the formation resistivity has a specific influence on DOD.

Investigation performance test of the optimized coil

To verify the detection ability of the optimized coils, three formation models (Fig. 13), namely single boundary (a), double boundaries (b) and multi-boundaries (c), are used to simulate the logging responses. It is essential to mention that the resistivity of the formation model is constant in the transverse direction. That is, there are no faults or other geological anomalies in the model.

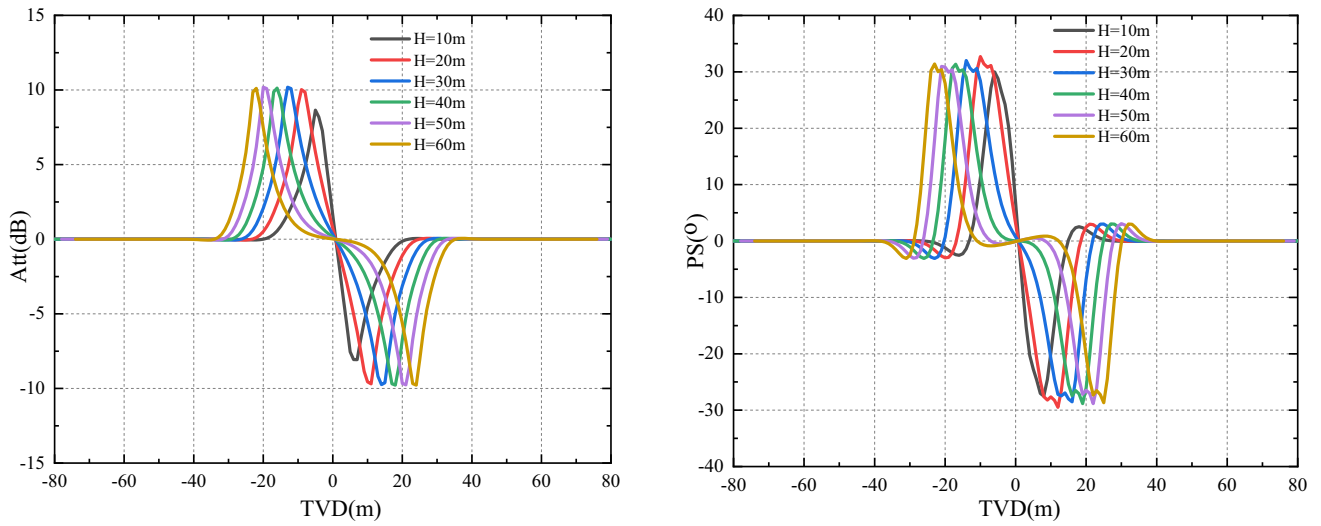


Fig. 11 Influence of formation thickness on Att and PS

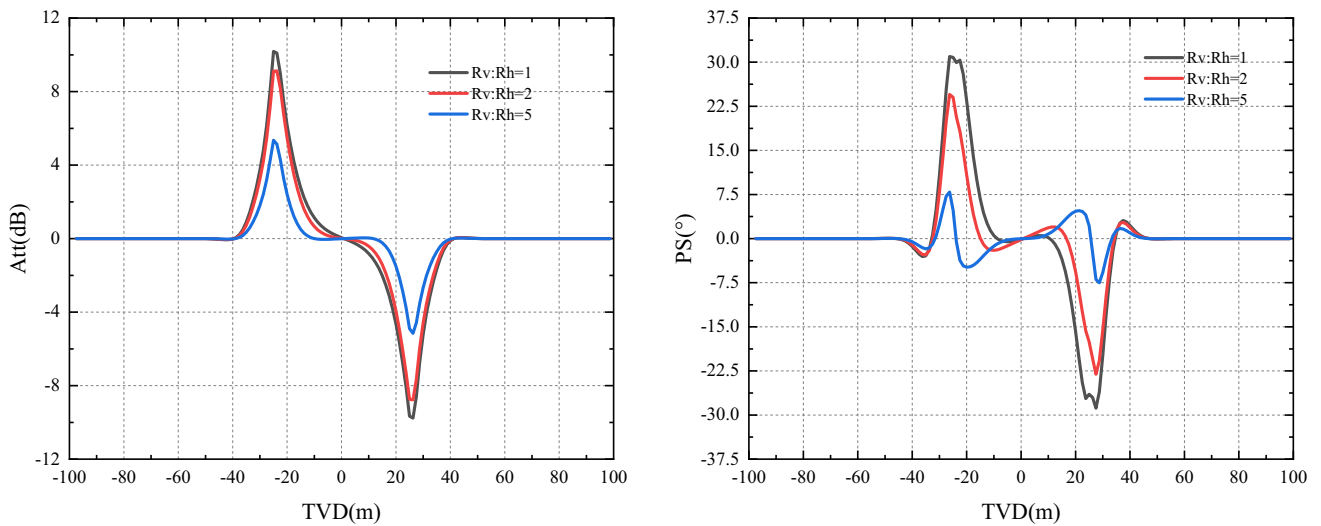


Fig.12 Influence of resistivity anisotropy on Att and PS

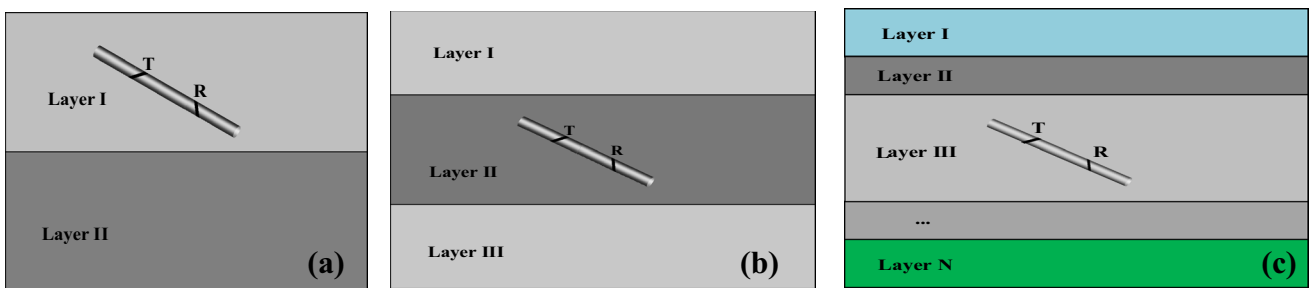


Fig. 13 Schematic diagram of the formation model with different boundaries

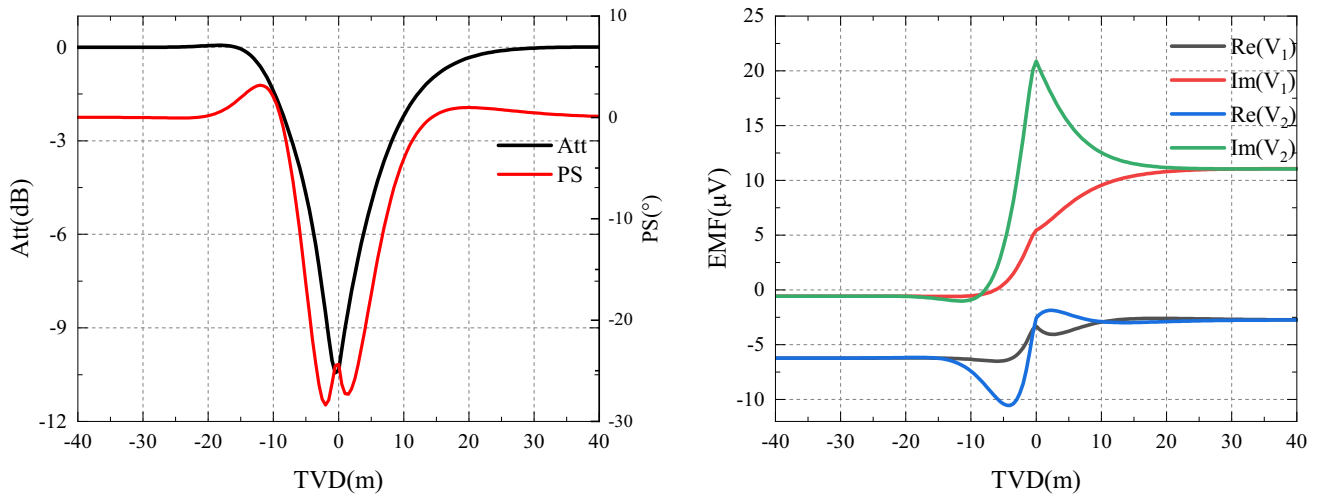


Fig. 14 Logging responses of a single boundary formation model

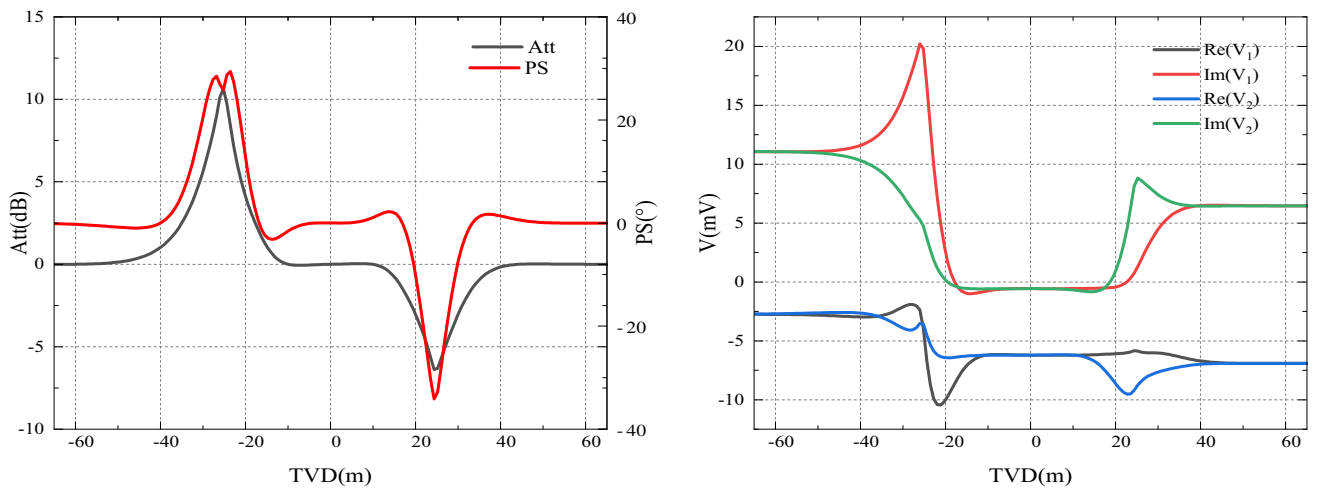


Fig. 15 Logging response of the dual boundaries formation model

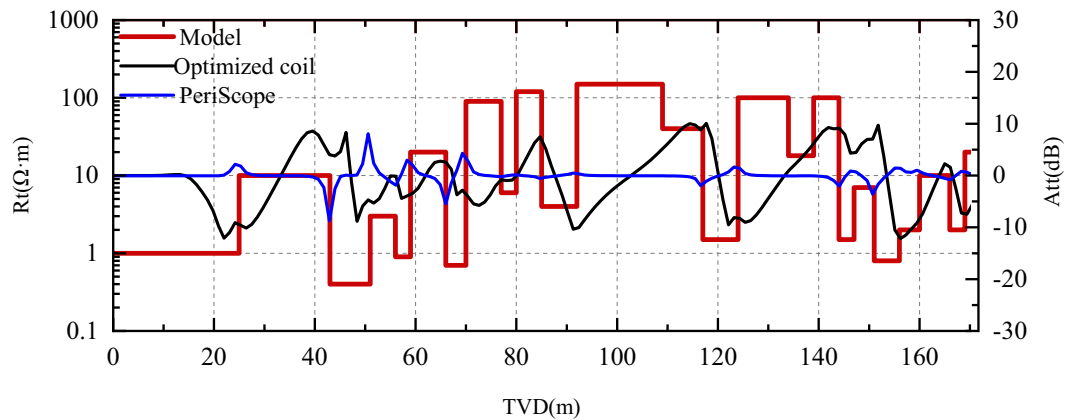


Fig. 16 The Att of optimized coils and PeriScope in Oklahoma formation

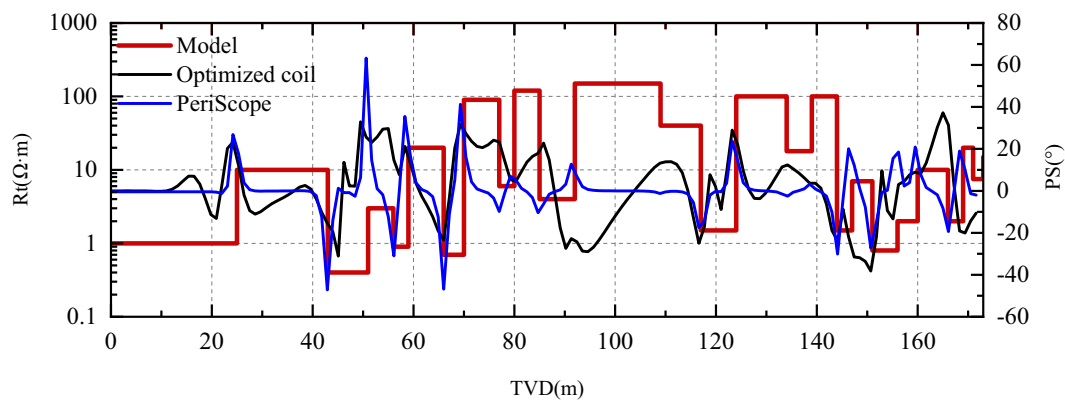


Fig. 17 The PS of optimized coils and PeriScope in Oklahoma formation

Single boundary

The model shown in Fig. 13a is used to test the logging response of the optimized tool in a single boundary. In the model, the upper layer is a low resistivity layer with $2 \Omega\cdot\text{m}$, while the lower layer is a high resistivity layer with $20 \Omega\cdot\text{m}$. The deviation angle of the well is 88° . In addition, the coordinate of the formation boundary is 0, and the turns of the transmitter and receiver are 100. Figure 14 presents the calculated measurement signal and the logging response of Att and PS, where V_1 and V_2 correspond to the measurement signals with azimuth angles of 0° and 180° , respectively. It can be seen that both the real part and the imaginary part of the EMF reach μV level. Thus, the signal of the optimized coils can be easily detected. Simultaneously, Att and PS responses can accurately determine the position of the formation boundary. When the tool enters the low resistivity formation from the high resistivity formation, the DOD of Att is 30 m while the DOD of PS is 33 m. When the tool enters the high resistivity formation from the low resistivity formation, the DOD of Att and PS are 22 and 19 m, respectively. It demonstrates that the DOD of the tool is much higher when the tool is in high resistivity formation to detect low resistivity formation.

Double boundaries

The logging response of the optimized coils in the dual boundaries formation is evaluated using the model shown in Fig. 13b. The resistivity of the middle layer is $2 \Omega\cdot\text{m}$. The resistivity of the upper and lower formations is 20 and $5 \Omega\cdot\text{m}$, respectively. The well deviation angle is 88° . Consequently, when the tool enters the middle formation from the upper formation or the lower formation, it belongs to the case that the tool in high resistivity formation to detect the low resistivity formation. The calculation results of

Fig. 15 demonstrate that the EMF can reach μV level. It also indicates that the DOD of Att is, respectively, 30 and 21 m, while the DOD of PS is 34 and 18.5 m, respectively, when the tool enters the lower formation from the upper formation and is close to the two boundaries. When the tool enters the upper formation from the lower formation and approaches the two boundaries, the DOD of Att is 17 and 17 m, while the DOD of PS is 18.5 and 21 m, respectively. The results show that the tool also has a high DOD in the double boundary formation. In addition, DOD will change due to the influence of the resistivity of the upper and lower formations.

Multi-boundaries

To compare the logging responses of the optimized coils and mature tools in multiple layers, a 25-layer Oklahoma formation model with a thickness of 170 m is developed. The coil with the lowest frequency of 100 kHz and spacing of 96 is considered in PeriScope tool. The coil structure is similar to that of the coil type I. Figures 16 and 17 display Att and PS responses, respectively. It can be seen that, compared with the PeriScope, the optimized coils have a more excellent response to the formation boundary and it is easier to identify the formation boundary in advance. Therefore, the logging response of type III in a thick layer is variable. The PeriScope is better at identifying thin layers than the optimized coils. And its logging response tends to be constant in thick layers. In summary, the optimized coils proposed in the paper are mainly suitable for the boundary detection of thick formation. The coil structure designed in this paper is based only on the theoretical calculation results. To verify its practical application effect, it is suggested to add relevant physical models in the future.

Summary and conclusions

In this paper, the coil of the ultra-deep azimuthal electromagnetic resistivity Logging While Drilling tool is optimized by numerical simulation, and the critical frequency and spacing parameters are determined by ergodic calculation. The following conclusions can be drawn:

- The double inclined coil system is optimized by a numerical simulation method that is very economical and efficient. The optimized coils have a depth of detection of 30 m, as well as good adaptability in anisotropic formation.
- The conductivity of the drilling collar greatly affects the measurement signal, while permeability does not influence the measurement signal.
- The Att and PS responses of the tool are affected by the resistivity anisotropy and thickness of the formation, and then affect the depth of detection of the tool.
- The optimized coils have strong a signal intensity (reaching μV level) in single boundary formation and double boundaries formation.
- Compared with the current tool, the optimized coils can be much easier to identify the formation boundary ahead in multi-boundaries formation.

Acknowledgements The authors would like to thank Sinopec Research Institute of Petroleum Engineering for allowing us to use the data in this study. The helpful suggestions from the two anonymous reviewers are gratefully acknowledged.

Funding This research is sponsored by the National Natural Science Foundation of China (Program Nos. 41904112 and 42102350), Natural Science Basic Research Plan in Shaanxi Province of China (Program No. 2021JQ-590), Scientific Research Program Funded by Shaanxi Province Education Department (Program No. 21JK0836), and China Postdoctoral Science Foundation (Program No. 2022M711442).

Open Access This article is licensed under a Creative Commons Attribution 4.0 International License, which permits use, sharing, adaptation, distribution and reproduction in any medium or format, as long as you give appropriate credit to the original author(s) and the source, provide a link to the Creative Commons licence, and indicate if changes were made. The images or other third party material in this article are included in the article's Creative Commons licence, unless indicated otherwise in a credit line to the material. If material is not included in the article's Creative Commons licence and your intended use is not permitted by statutory regulation or exceeds the permitted use, you will need to obtain permission directly from the copyright holder. To view a copy of this licence, visit <http://creativecommons.org/licenses/by/4.0/>.

References

Anderson WL (1979) Computer programs numerical integration of related Hankel transforms of order 0 and 1 by adaptive digital filtering. *Geophysics* 44(3):1285–1305

- Bittar M, Klein J, Best R, Hu G, Wu M, Pitcher J (2007) A new azimuthal deep-reading resistivity tool for geosteering and advanced formation evaluation. In: SPE Annual Technical Conference and Exhibition.
- Gao J, Xu CH, Xiao JQ (2013) Forward modelling of multi-component induction logging tools in layered anisotropic dipping formations. *J Geophys Eng* 10(5):054007
- Hartmann A, Vianna A, Maurer H M, Sviridov M, Martakov S, Antonen F, Olsen P A, Constable M V (2014) Verification testing of a new extra deep azimuthal resistivity measurement. In: SPWLA 55th Annual logging symposium.
- Iverson M (2004) Geo-steering using ultra-deep resistivity on the Grane field Norwegian North Sea. In: SPWLA 44th annual logging symposium.
- Johansen HK, Sørensen K (1979) Fast hankel transforms. *Geophys Prospect* 27(4):876–901
- Li KS, Gao J, Ju XD, Zhu J, Xiong YC, Liu S (2018) Study on ultra-deep azimuthal electromagnetic resistivity LWD tool by influence quantification on azimuthal depth of investigation and real signal. *Pure Appl Geophys* 175(12):4465–4482
- Li H, Wang H, Wang L, Zhou XT (2020a) A modified Boltzmann Annealing Differential Evolution algorithm for inversion of directional resistivity logging-while-drilling measurements. *J Petrol Sci Eng* 188:106916
- Li KS, Gao J, Zhao X (2020b) Tool design of look-ahead electromagnetic resistivity LWD for boundary identification in anisotropic formation. *J Petrol Sci Eng* 184:106537
- Li Q M, Omeragic D, Chou L, Yang L, Duong K (2005) New directional electromagnetic tool for proactive geosteering and accurate formation evaluation while drilling. In: SPWLA 46th annual logging symposium.
- Omeragic D, Li Q, Yang L, Duong K, Smits J, Liu B C, Yang J (2005) Deep directional EM measurements for optimal well placement. In: SPE annual technical conference and exhibition.
- Oystein B, Vikhamar P, Spotkaeff M, Dolan J, Wang H F, Ceyhan A (2014) Shine a light in dark places using deep directional resistivity to locale water movement in Norway oldest field. In: SPWLA 55th annual logging symposium.
- Prensky S (2006) Recent advance in LWD and formation evaluation. *World Oil* 227(3):69–74
- Rabinovich M, Le F, Lofts JJ, Martakov S (2012) The vagaries and myths of “Look Around” deep-resistivity measurements while drilling. *Petrophysics* 53(02):86–101
- Rabinovich M, Le F, Lofts J J, Martakov S (2011) Deep? how deep and what? the vagaries and myths of look around deep-resistivity measurements while drilling. In: SPWLA 52nd annual logging symposium.
- Seydoux J, Legendre E, Mirto E, Dupuis C, Denichou J M, Bennett N, Kutiev G (2014) Full 3D deep directional resistivity measurements optimize well placement and provide reservoir-scale imaging while drilling. In: SPWLA 55th annual logging symposium.
- Thiel M., Dzevat O (2018) Azimuthal imaging using deep-directional resistivity measurements reveals 3D reservoir structure. In: SPWLA 59th Annual Logging Symposium.
- Wang L (2018) Deep-exploration multi-component Logging While Drilling electromagnetic logging: theory, forward modeling and inversion/data processing, China University of Petroleum (East China).
- Wang T (2008) Method of generating a deep resistivity image in LWD measurements, US Patent, 1–17.
- Wei BJ, Ou YF, Wu Y, Wang SS (2012) Simulation of tilted coil's response in cylindrically stratified media and its application for electromagnetic propagation measurement while drilling. *J China Univ Petrol (edition of Natural Science)* 36(5):72–79

- Wei BJ, Tian K, Zhang X, Liu K (2010) Physics of directional electromagnetic propagation measurements-while-drilling and its application for forecasting formation boundaries. *Chin J Geophys-Ch* 53(10):2507–2515
- Wu YM, Xiong SQ, Li CY, Fang YJ, Baker H (2013) Application of AziTrak tool to geosteering of horizontal well development. *Well Logging Technol* 05:547–551
- Wu ZG, Wang L, Fan YR, Deng SG (2020) Detection performance of azimuthal electromagnetic logging while drilling tool in anisotropic media. *Appl Geophys* 17(1):1–12
- Wu H H, Golla C, Parker T, Clegg N, Monteilhet L (2018) A new ultra-deep Azimuthal Electromagnetic LWD sensor for reservoir insight. In: SPWLA 59th Annual logging symposium.
- Zhang P, Deng SG, Hu XF, Wang L, Wang ZK, Yuan XY, Cai LY (2021) Detection performance and sensitivity of logging-while-drilling extra-deep azimuthal resistivity measurement. *Chin J Geophys-Ch* 64(6):2210–2219
- Zhang ZY, Gonget C, Raian V, Roeterdink R (2008) Directional LWD resistivity tools and their business impacts. In: SPWLA 49th annual logging symposium.

Publisher's Note Springer Nature remains neutral with regard to jurisdictional claims in published maps and institutional affiliations.